ECS Transactions, 78 (1) 795-805 (2017)
10.1149/07801.0795ecst ©The Electrochemical Society

Study of the Rate Limiting Steps and Degradation of a GDC Impregnated $La_{0.6}Sr_{0.4}Co_{0.8}Fe_{0.2}O_{3-\delta}$ Cathode

J. Ascolani-Yael[a], A. Montenegro-Hernández[a,b], H. Troiani[a,b], L. Mogni[a,b], A. Caneiro[b]

[a]Centro Atómico Bariloche (CAB) – Comisión Nacional de Energía Atómica (CNEA)
Av. Bustillo 9500 S.C. de Bariloche, CP 8400, Argentina
[b]Consejo Nacional de Investigaciones Científicas y Técnicas (CONICET)
Av. Rivadavia 1917 (C1033AAJ), Buenos Aires, Argentina

In this work, a Solid Oxide Fuel Cell (SOFC) cathode surface modification by nanoparticle impregnation was carried out. $La_{0.6}Sr_{0.4}Co_{0.8}Fe_{0.2}O_{3-\delta}$ (LSCF) ceramic cathodes impregnated with $Ce_{0.8}Gd_{0.2}O_{3-\delta}$ (GDC) nanoparticles were characterized with scanning (SEM) and transmission (TEM) electron microscopy. The electrochemical response as a function of temperature, oxygen partial pressure (pO_2) ($10^{-4} < pO_2 < 1$ atm) and time was evaluated by electrochemical impedance spectroscopy (EIS). We obtained reproducible and homogeneous impregnations, which reduce the total cathode´s polarization resistance more than 20% in the temperature range between 400ºC and 800ºC and during 500 h at 700ºC. The impregnated cathode was found to be electrochemically limited by the same processes as the non-impregnated cathode, namely gas diffusion, ion bulk diffusion and dissociative adsorption. The impregnation produced a reduction of more than 20% of the oxygen surface resistance; such difference remained stable through 500h of continuous operation at 700ºC.

Introduction

Solid oxide cells (SOCs) are ceramic devices that transform chemical energy into electrical energy (SOFC mode) or electrical energy and heat into fuel production (SOEC mode) without running out of energy, as long as fuel or energy is provided, depending on the mode being used. Diverse fuels can be used in SOFC mode, between them methane and hydrogen, for producing electrical energy. High purity fuels can be produced (such as H_2) using the cells in SOEC mode, providing the cell with electrical energy. The cells efficiency is mainly limited by the polarization losses associated to ohmic and electrochemical processes, such as oxygen reduction reaction (ORR) at the cathode. The cathode polarization resistance is especially important as operation temperature decreases. This is a big challenge since much effort is being made towards lowering the operation temperatures to below 700ºC (IT-SOFC) to reduce, among other things, the different cell components degradation (1).

One adopted strategy to decrease the cathode polarization resistances, which has generated considerable expectation, is the cathode's surface modification through the so called “wet impregnation technique” (2,3). This approach consists in synthesizing a catalyst material (which can be a metal, another electrode material, an ion-conducting

material or a MIEC) on top of an already electrochemically-active electrode's surface. This technique broadly consists of wetting the electrode with a catalytic precursor solution followed by a heat treatment, which usually requires a lower synthesis temperature than the heat treatment used to synthesize the electrode material. Historically, the impregnated materials used were Pt, Pd, Ag, which are well known catalysts, but present disadvantages such as the economic cost (4,5).

Currently, other materials with different ionic and electronic properties are being investigated as impregnations in order to reach good catalytic and stability properties, mainly oxides already used as electrodes or electrolytes. For example, a reduction of the ORR resistance has been reported impregnating $Ce_{0.8}Gd_{0.2}O_2$ into $(La_{0.8}Sr_{0.2})_{0.9}MnO_3$ (LSM) (6), $Sm_{0.2}Ce_{0.8}O_{1.9}$ into $La_{0.85}Sr_{0.15}MnO_{3-\delta}$ (7), $Sm_{0.2}Ce_{0.8}O_{1.95-\delta}$ into $La_{0.6}Sr_{0.4}Co_{0.2}Fe_{0.8}O_{3-\delta}$ (8), $Sm_{0.5}Sr_{0.5}CoO_{3-\delta}$ into $La_{0.6}Sr_{0.4}Co_{0.2}Fe_{0.8}O_{3-\delta}$ (9) and many other configurations (2,3).

The mechanisms through which impregnation reduces polarization resistances (R_{pc}) in this approach is still under debate. It has been proposed that the increase in the TPB's length is not enough to account for the reduction in the polarization resistance, proposing that a complex interaction between the scaffold and the impregnated material on the surface of the electrode, which would raise oxygen surface exchange coefficient, would be the cause for the reduction. Alternatively, Yildiz et al. (10) have proposed that mechanical stretching could affect local oxygen vacancy concentrations, modifying the exchange rate coefficients.

$La_{0.6}Sr_{0.4}Co_{0.8}Fe_{0.2}O_{3-\delta}$ (LSCF) is a perovskite structured oxide which is a candidate to be used as a cathode for intermediate solid oxide cells (IT-SOC) due to its properties as a mixed conductor (11). In this material, the ORR is controlled by O-ion bulk diffusion when the particle size is micrometric (12) and by O-ion bulk diffusion and O-surface exchange reaction when the cathode is nano-structured (13).This work presents a study about how the surface modification of LSCF electrodes by $Ce_{0.8}Gd_{0.2}O_2$ (GDC) nanoparticles impregnation affects the cathode polarization resistance and its time evolution. The aim of this work is to rationalize the effect of surface modification on the ORR and degradation mechanism.

Experimental

Symmetrical Cells Preparation

LSCF powder was obtained by a chemical method involving a gel formation by polymerization of Acetyl-Acetone (AcAc) and Hexamethylenetetramine (HMTA)(11). Stoichiometric proportions of La_2O_3, $SrCO_3$, $Co(CH_3COO)_2$ and $Fe(CH_3COO)_2$ were dissolved in acetic acid, and HMTA, AcAc and hydrogen peroxide were added, all in a concentration ratio to cations of 3:1. The solution was then slowly dried, forming a solid gel, followed by calcination at 400°C for 1h. The resulting powder was ball-milled and ultimately heat treated at 1000°C for 4h. $La_{0.8}Sr_{0.2}Ga_{0.8}Mg_{0.2}O_{3-\delta}$ (LSGM) commercial powders (Fuel Cells Materials-Nexceris) were uniaxially pressed and sintered at 1450°C for 6h, obtaining dense electrolytes. LSCF ink was prepared using isopropyl alcohol, alpha-terpineol, polyvinyl butyral (PVB), polyvinyl pyrridone (PVP) and LSCF in a

weight ratio of 38.8:23.6:1.7:0.9:35. The LSCF ink is then deposited on the LSGM electrolytes using the spin coating technique, and calcined at 1000ºC during 1h, obtaining symmetrical cells with porous LSCF electrodes of approximately 18μm.

Impregnation

Afterwards, the symmetrical cells were impregnated with a Ce and Gd nitrate solution, of concentration 0.048M and 0.012M, respectively. Water and ethanol were used as solvents in a 0.5:0.5 volume ratio. UREA (in a 5:2 molar ratio to the final GDC desired quantity) was used as a surfactant. Ethanol is added to the impregnating solution in order to decrease the surface tension, allowing the solution to wet the LSCF better and also helping in forming more spatially homogeneous distributed particles. On the other hand, UREA controls the particle forming during the sol gel process, helping the phase formation and promoting more uniform sized particles (14). The solution was dropped on the porous LSCF electrode allowing each drop to dry before dropping the next one. The total volume of solution deposited was such that the final quantity of GDC synthesized on each side of the cell was approximately 10% of the electrode mass. The impregnated cell was heat treated at 800°C for 1h, in order to synthesize the GDC nanoparticles. Ag conductive paint was used as current collectors.

Sample Characterization

All samples were characterized before and after the electrochemical testing. Microstructure was studied with a FEG-SEM (FEI Nova NanoSEM 230) microscope using 5kV acceleration voltage in order to follow the micro structural changes suffered by the samples in each stage of the experiment. The impregnated particles and the interfaces were also analyzed with TEM (Philips CM 200 UT). The crystal structure was analyzed by XRD, using a Panalytical-Empyrean diffractometer, with Cu K_α radiation.

Electrochemical Measurements

Electrochemical Impedance Spectroscopy (EIS) was used to study the mechanism of the oxygen reduction reaction and to evaluate the time evolution of the polarization resistance (R_{pc}) of the samples. These measurements were performed with a frequency response analyzer (FRA) coupled to an AUTOLAB potentiostat, measuring between 0.2 mHz and 1MHz, with 50mV of amplitude and 0V of bias potential.

The measurements varying temperature were made each 100°C by increasing temperature from 400°C to 800°C under synthetic air flow (Ar- O_2 and He – O_2). The measurements varying oxygen partial pressure were made mixing O_2 and Ar (or He), with a total gas flow of 100mL/min, by means of an electrochemical pump and monitored with an oxygen gauge (15).

The time evolution measurements were made at 700°C in air for 500h in air. All impedance spectra were fitted using ZView with a series combination of an inductance, a resistance, an extended element (DX11 in ZView, Transmission Line Model) and a RCPE circuit (composed of a resistance R in parallel with a Constant Phase Element (Cpe)). We used the Transmission Line Model to model the cathode reaction based on the work by Baqué et al. (13), in which this model is used to fit the impedance spectra of

$La_{0.6}Sr_{0.4}Co_{0.2}Fe_{0.8}O_{3-\delta}$. The TLM is based on the well-known Adler-Lane-Steele model, which describes a finite length MIEC electrode reaction.

Results and Discussion

Sample Characterization

Figure 1a) shows SEM images of an LSCF sample and Figure 1b) a 10% GDC impregnated LSCF sample. Figure 1a) shows that LSCF grain size is roughly about 100-200nm while Figure 1b) shows the LSCF grains with a homogeneous GDC impregnation, with particles of about 15nm in size. A similar particle size and a spatially homogeneous distribution were observed all throughout the samples.

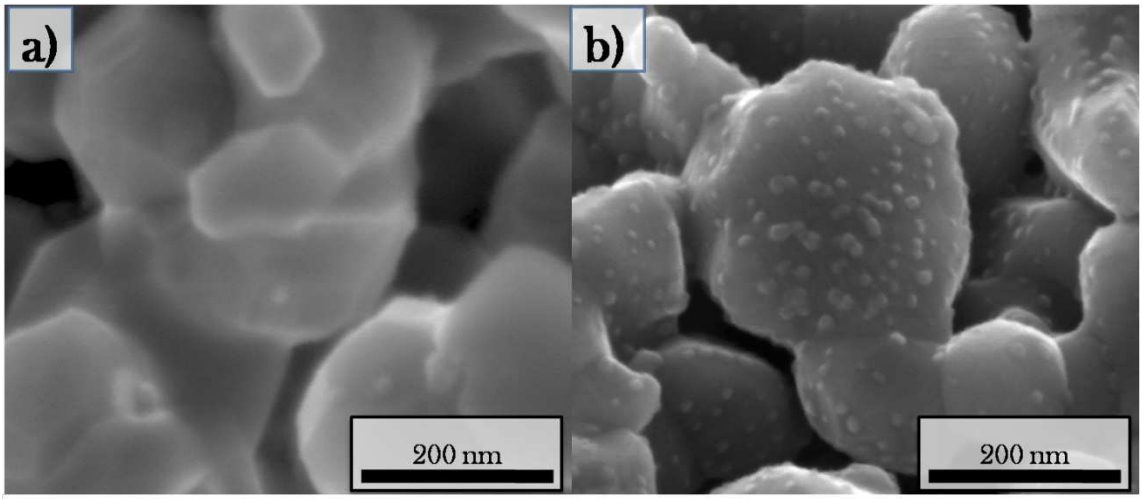

Figure 1. SEM image of: a) non impregnated LSCF and b) LSCF impregnated with 10% GDC. The ~ 15nm particles are GDC and the ~ 200nm ones are LSCF.

Figure 2a) shows a typical XRD pattern of an LSCF sample and a 10% GDC impregnated LSCF sample. LSCF has a perovskite structure with a lattice parameter a = 3.86Å in agreement with Wang (16) and GDC has fluorite crystal structure with a lattice parameter a = 5.42Å (17). The peaks at 28.5° and 56° - that correspond to the (111) and (311) reflections - allow the identification of the GDC phase, while all the others correspond to LSCF or both GDC and LSCF. This diffraction pattern indicates the absence of other phases in the sample. On the other hand, Figure 2b) shows a HR-TEM image of a GDC particle (right) on the surface of a LSCF particle (left). The lattice parameters were obtained calculating the Fast Fourier Transform (FFT) of the squared regions. The planes observed correspond to the [111] of GDC and the [110] of LSCF. The lattice parameters obtained from these are: a = 5.42Å and a = 3.83Å; which belong to the GDC and LSCF lattice parameters respectively, a result that coincides with XRD data.

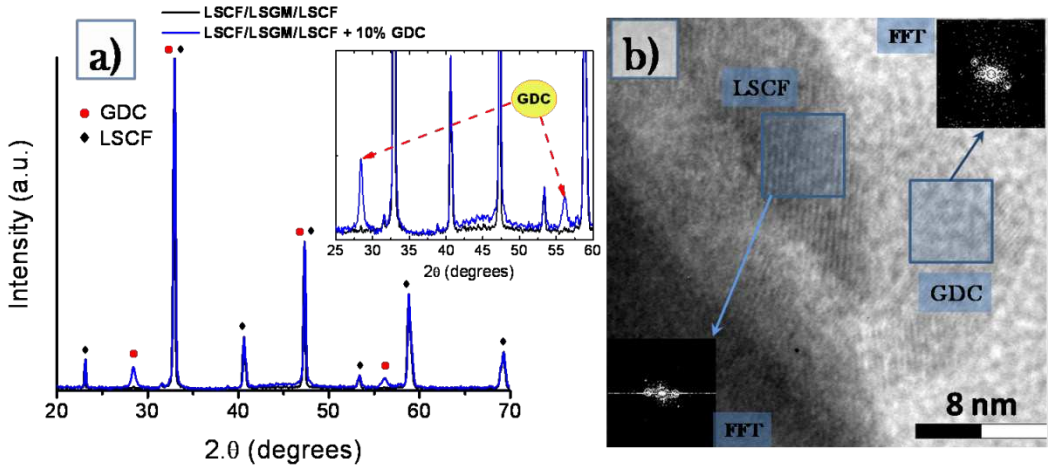

Figure 2. a) XRD pattern of the non-impregnated LSCF sample (black) and the impregnated sample (blue). The red dots indicate the peaks which belong to LSCF and the black diamonds indicate the peaks corresponding to GDC. b) TEM image of a GDC impregnated LSCF sample. The violet squares show were the FFT has been calculated and the black squares in the corners are the resulting FFTs.

Reaction Mechanism and Impregnation´s Influence

Figure 3a) and 3b) show typical Nyquist and Bode plots, respectively. The spectra correspond to an impregnated and non-impregnated cell measured at pO_2 = 0.013atm and at 700ºC, each one using Ar and He as gas carriers. The electrolyte resistance was subtracted in order to make the cathodes comparison easier. All spectra are formed of at least two arcs, centered in different frequencies. The high frequency arc (~ 30 Hz) looks almost the same for the four spectra while the low frequency arc (centered at about 0.3-0.15Hz) changes, showing a clear reduction of the resistance values between the non-impregnated and the impregnated cathode. Also, a similar effect is seen changing from using Ar to He as gas carriers.

The difference between the measured R_{pc} of the same sample in Ar and He is attributed to the difference between the diffusion coefficient of O_2 in Ar and O_2 in He. Therefore it can be assumed that gas diffusion is one of the rate limiting steps involved (especially at low pO_2 and high temperature), and the usual RCPE circuit can be used to model this process (12). However, the reduction of the low frequency arc is less than expected if it were only due to oxygen gas diffusion. In such a case, the reduction expected for changing from Ar to He as gas carriers is a reduction of about one fifth. This discrepancy indicates that the low frequency response involves more than one arc. Then, besides the O_2 gas diffusion, and in agreement with literature (18), the high frequency response is modeled by Transmission Line Model, which is based on the well-known Adler-Lane-Steele model for mixed electronic and ionic conductors – MIECs –. This response involves O-ion bulk diffusion and surface reaction as co-limiting processes.

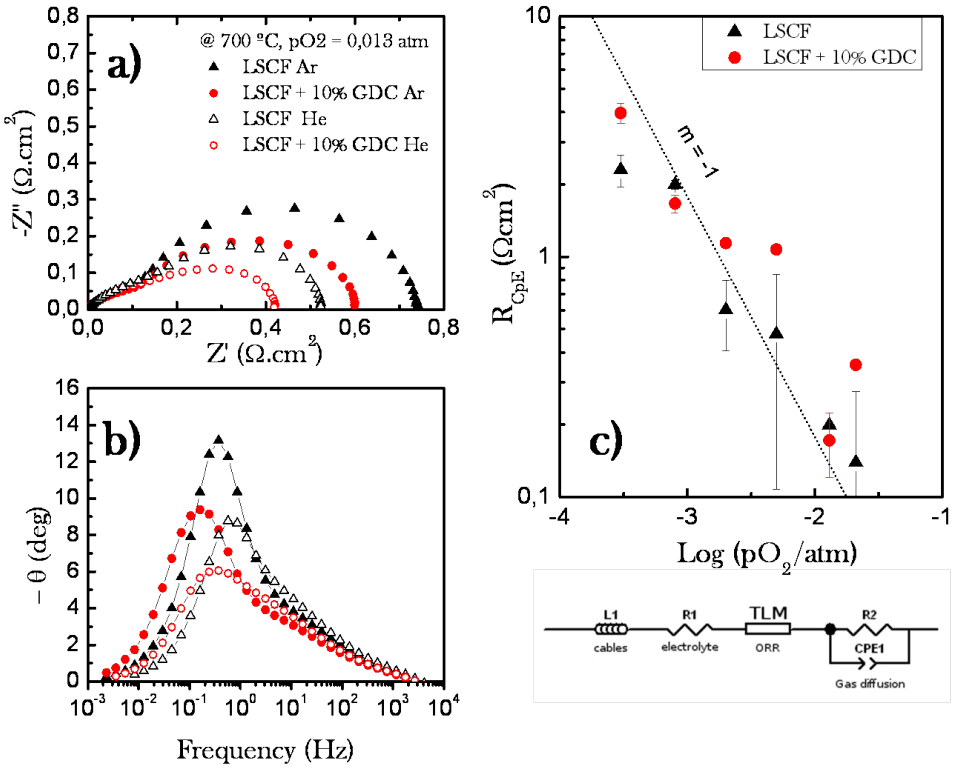

Figure 3. a) Nyquist and b) Bode plots of EIS measurements of a non-impregnated LSCF cathode and a 10% GDC impregnated LSCF cathode, both measured using Ar and He as O_2 gas carriers. c) Polarization resistance of the RCPE circuit (R_{CPE}) as a function of pO_2, for measurements performed in Ar. The electrical equivalent circuit used to fit the EIS measurements is also included.

Taking into account the previous discussion, all EIS spectra were fitted using the electrical equivalent circuit shown in Figure 3, in which L1 represents the inductance of the wires, R1 represents the electrolyte resistance, R2 a resistance and CPE1 a constant phase element. The element TLM represents the cathode reaction itself, it´s impedance is derived from the Adler-Lane-Steele model and it´s expression for a MIEC cathode is shown in Equation [1] (13, 19).

$$Z = \sqrt{r_{bulk}.r_{surf}}\sqrt{\frac{1}{1+r_{surf}.q_{surf}.j.\omega}}.coth\left(L\sqrt{\frac{r_{bulk}}{r_{surf}}}\sqrt{1+r_{surf}.q_{surf}.j.\omega}\right) \quad [1]$$

where L is the cathode thickness (determined from SEM images), r_{bulk} is a distributed resistance which describes the O-ion diffusion through the bulk, $r_{surf,}$ and q_{surf} are the parameters of a RCPE circuit, which are a distributed resistance and a distributed capacitance describing the oxygen surface exchange reaction, respectively. r_{bulk} ,r_{surf}, and q_{surf} are the fitted parameters. From the values of r_{bulk} and r_{surf}, the cathode´s bulk ionic resistance -R_{bulk} ($\Omega.cm^2$)-and the cathode´s surface resistance -R_{surf} ($\Omega.cm^2$)- can be obtained by making the following operations, in which A denotes the sample transversal area:

$$R_{bulk} = A.Lr_{bulk} \quad \text{and} \quad R_{surf} = A.r_{surf}/L \quad [2]$$

Figure 3c) shows the variation of the fitted R_{CPE} values with pO_2, in which the observed slope is m ~ -0.7. This value is slightly lower than the expected for a gas diffusion process (i.e. m = -1) (20), but considering the errors from fitting, the high capacitance values and the reduction of the R_{CPE} when Ar is changed by He as gas carrier, it can be assumed that this contribution is due to O_2-gas diffusion.

Figure 4a) shows the dependence of the values of the TLM fitted parameters with oxygen partial pressure. Both impregnated and non-impregnated cathodes have very little variation of the oxygen bulk diffusion, described by R_{bulk}. This result was expected, due to the low dependency of the oxygen vacancy concentration with pO_2 in LSCF (12, 13). On the other hand, the impregnated and non-impregnated cathodes have a dependency of R_{surf} with pO_2, which is described by a slope m= -0.5 ~ -0.6, the expected value for surface dissociative adsorption (21). The absolute values difference of the surface resistance for the impregnated cathode is at least 20% below the non-impregnated one for all measured pressures, though this is not clearly visible due to the logarithmic scale. Therefore, the main effect of impregnation is to reduce the surface dissociative adsorption polarization resistance.

TABLE I. TLM fitting results.

Slope –m-	**vs t ($\Omega.cm^2.h^{-1}$)**		**vs pO_2**		**vs T =E_{act} (eV)**	
	LSCF	LSCF + 10%GDC	LSCF	LSCF + 10%GDC	LSCF	LSCF + 10%GDC
R_{tot}	$1.94.10^{-4}$	$1.43.10^{-4}$	-	-	-	-
R_{surf}	7.10^{-4}	5.10^{-5}	-0.6	-0.6	1.13	1.16
R_{bulk}	$4.4.10^{-4}$	$3.9.10^{-4}$	-0.02	-0.07	1.26	1.24
R_{CPE}	-	-	-0.7	-0.7	-	-

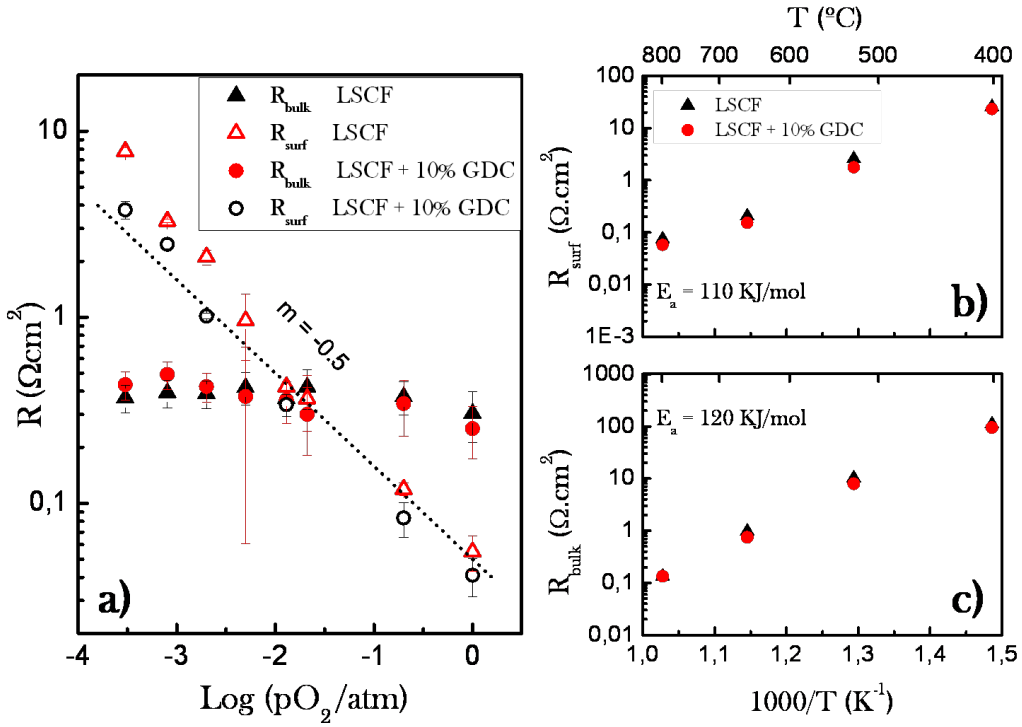

Figure 4. a) Bulk (R_{bulk}) and surface (R_{surf}) resistances values for the impregnated and non-impregnated cells as a function of pO_2. Arrhenius plot of b) R_{surf} and c) R_{bulk}.

Figure 4b) and 4c) show the dependence of R_{surf} and R_{bulk} with temperature. Despite the surface modification by impregnation seems to affect the surface reaction decreasing its resistance, no change in activation energy for R_{surf} was observed between the samples. This is also the case for R_{bulk}, where no change in the activation energy is observed. It can be noted that the values obtained for R_{bulk} are in agreement with the values found in bibliography where, for example, Wang calculated an ionic resistivity from diffusivity data of $\rho = 25\Omega.cm$ at 800ºC (16), which results a $R_{bulk} \sim 0.05\Omega.cm^2$ for an electrode of 18µm.

Time Evolution of Cathode and Impregnation´s Influence

In order to study the degradation mechanisms of the impregnated and non-impregnated samples, EIS spectra were acquired during 500h of continuous operation at 700ºC in air. The left panel of Figure 5 shows the total cathode polarization resistance (R_{pc}) as a function of time, where the R_{pc} of the impregnated sample is always lower than the non-impregnated one, and its velocity of degradation is also smaller, especially after 300h of operation.

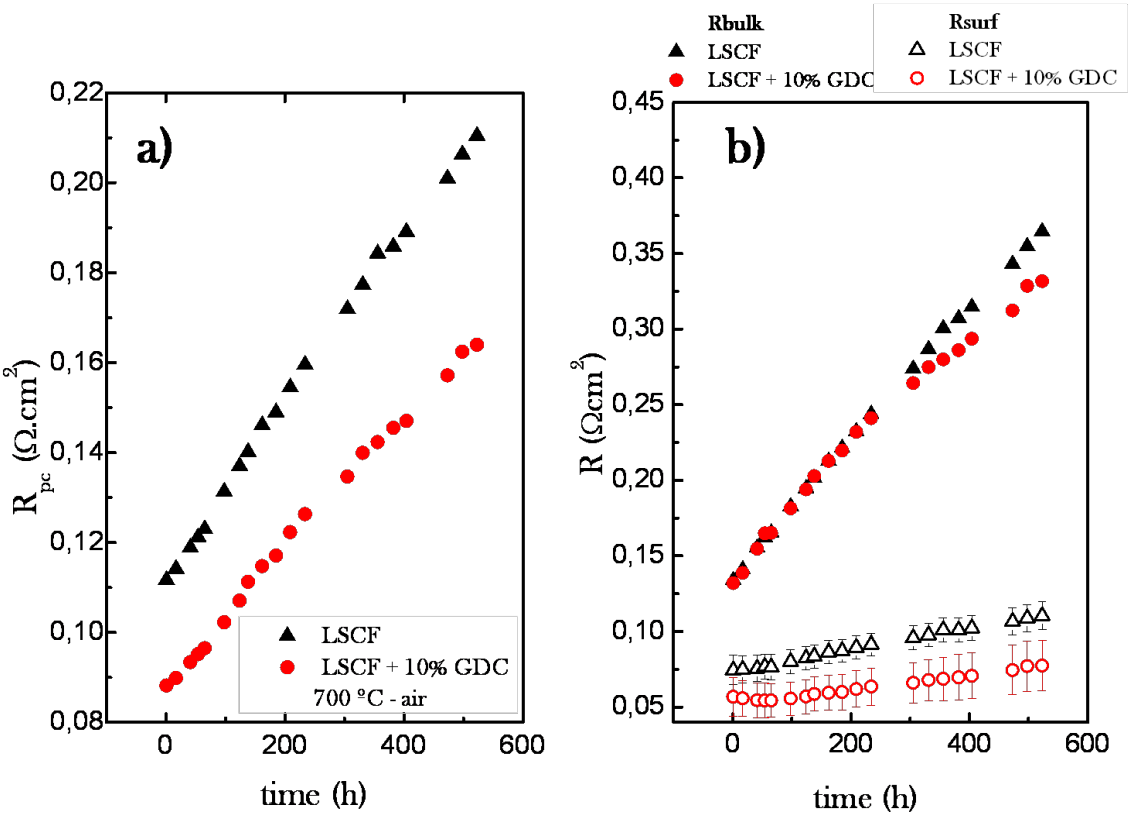

Figure 5. a) total electrode polarization resistance values for the impregnated and non-impregnated samples, measured during 500h at 700°C with 100mL/min air flow. b) time evolution of the bulk (R_{bulk}) and surface (R_{surf}) resistances.

In the right panel of Figure 5 the fitted values for the TLM model are shown, in which R_{bulk}, the ionic conduction resistance in LSCF, is almost the same for the impregnated and non-impregnated samples, up to 300h of continued operation. From there on, the impregnated sample reduces its degradation velocity giving rise to the slight slope change observed in the total cathode polarization resistance. Meanwhile, the surface resistance of

the impregnated cathode – R_{surf}– is always at least 20% lower, and also has a 29% lower slope value, in comparison with the non-impregnated one. This is a stable effect and it is clear it is produced by the GDC impregnation.

In both cases, R_{surf} has a lower absolute value than R_{bulk} and also grows more slowly than R_{bulk} (see slopes in Table 1).

Figure 6a) shows a SEM image of the GDC impregnated sample after the time evolution test. It is clearly seen that the nanometric particles are not present anymore. On the other hand, in Figure 6b), a shift in the 28.5º XRD reflection of GDC phase of the same impregnated sample can be observed, before and after the aging test. From the XRD measurements (the full scale pattern is not shown) it is clear that, although not visible with SEM, GDC is still present and that there is a shift to a higher angle. There is also intensity loss after 500h of operation at 700ºC, taking the 33º LSCF reflection intensity as a reference. The shift in angle means the lattice parameter changed from a = 5.42Å to a = 5.37Å, while the loss of relative intensity indicates the dissolution of the GDC phase after the EIS measurements. These changes can be an evidence of cation inter-diffusion between LSCF and GDC phases.

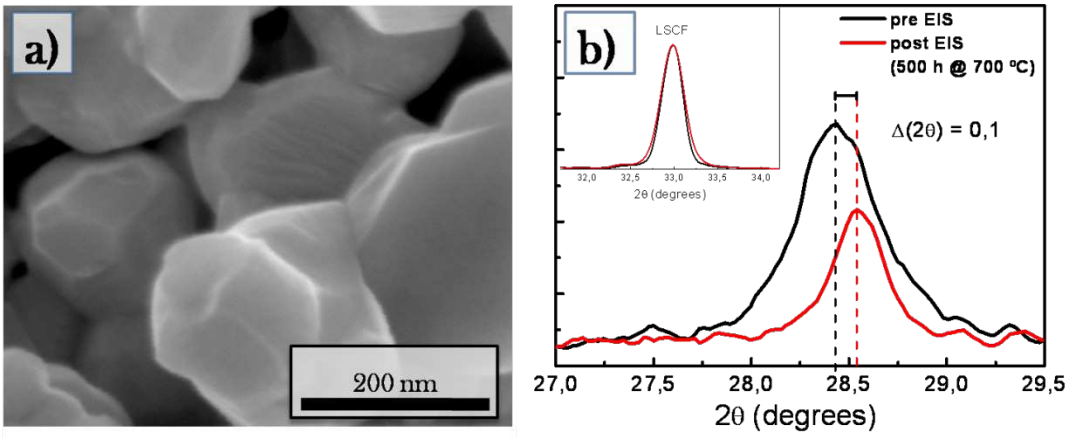

Figure 6. a) SEM image of the GDC impregnated LSCF sample, taken after the time evolution EIS measurements –i.e. 500h at 700ºC-. (see Figure 1b) for comparison). b) XRD reflection (~28.5º) of GDC impregnated phase before and after the EIS measurements. The inset shows the main peak of LSCF at 33º, which shows no shift in angle.

While notorious changes are observed especially with SEM and, in less proportion, with XRD after the EIS measurements, in the EIS measurements the only change is seen after 300h in R_{bulk}. Izuki *et al* have observed La diffusion into GDC and diffusion of Ce and Gd into LSCF in inter-diffusion experiments (22). If this were the case in our experiments, these processes might help to explain the change in lattice parameters, the "melting" of particles and the change in R_{bulk}, although this is speculation so far.

Conclusions

LSCF cathodes were decorated with 10% of GDC nanoparticles by the wet impregnation method. A spatially homogeneous impregnation, a reasonable size distribution and good sample reproducibility were achieved by using ethanol and water as

solvents with UREA as surfactant to make the impregnation solution. Through EIS measurements, a reduction of more than 20% of the total cathode polarization resistance was observed, and varying pO_2 we found the rate limiting mechanisms are ion bulk diffusion, dissociative adsorption reaction and gas diffusion. We also found the initial effect of the impregnation is to lower the dissociative adsorption resistance. The activation energies of each mechanism were measured varying temperature, were no difference between the impregnated and non-impregnated samples was observed. Time evolution measurements were made during 500h at 700ºC in order to study the impregnation stability. While it can be observed that the GDC particles disappeared, the GDC phase is still present with a small decrease of its lattice parameter. EIS measurements show, comparing with the degradation of non-impregnated LSCF, no changes in dissociative adsorption resistance degradation but show a small change in bulk ion diffusion resistance degradation. A detailed study of the mechanisms which produce the observed changes of the impregnations microstructure, lattice parameter and ion bulk diffusion degradation is needed in order to understand and control the degradation of an impregnated cathode.

Acknowledgments

The authors acknowledge the financial support of CNEA, CONICET. We also acknowledge for SEM technical support provided by M. Cortés and P. Troyón.

References

1. Z. M. Gao, Liliana Veronica, Elizabeth C. Miller, Justin Gary Railsback, Scott Barnett, *Energy & Environmental Science*, In Press (2016).
2. S. P. Jiang, *International Journal of Hydrogen Energy*, **37**, 449 (2012).
3. D. Ding, X. Li, S. Y. Lai, K. Gerdes and M. Liu, *Energy & Environmental Science*, **7**, 552 (2014).
4. Y. Sakito, A. Hirano, N. Imanishi, Y. Takeda, O. Yamamoto and Y. Liu, *Journal of Power Sources*, **182**, 476 (2008).
5. F. Liang, J. Chen, J. Cheng, S. P. Jiang, T. He, J. Pu and J. Li, *Electrochemistry Communications*, **10**, 42 (2008).
6. S. P. Jiang and W. Wang, *Journal of The Electrochemical Society*, **152**, A1398 (2005).
7. L. Zhang, F. Zhao, R. Peng and C. Xia, *Solid State Ionics*, **179**, 1553 (2008).
8. L. Nie, M. Liu, Y. Zhang and M. Liu, *Journal of Power Sources*, **195**, 4704 (2010).
9. X. Lou, S. Wang, Z. Liu, L. Yang and M. Liu, *Solid State Ionics*, **180**, 1285 (2009).
10. B. Yildiz, *MRS Bulletin*, **39**, 147 (2014).
11. L. Baqué, A. Caneiro, M. S. Moreno and A. Serquis, *Electrochemistry Communications*, **10**, 1905 (2008).
12. N. Grunbaum, L. Dessemond, J. Fouletier, F. Prado, L. Mogni and A. Caneiro, *Solid State Ionics*, **180**, 1448 (2009).
13. A. L. S. Laura C. Baque, Erico Teixeira-Neto, Horacio E. Troiani, Anja Schreiber, Adriana C. Serquis, *Journal of Power Sources*, **337**, 166 (2017).

14. Z. L. Xiaoyuan Lou, Shizhong Wang, Yonghao Xiu,, C. P. Wong, Meilin Liu, *Journal of Power Sources*, **195**, 419 (2010).
15. A. Caneiro, P. Bavdaz, J. Fouletier and J. P. Abriata, *Review of Scientific Instruments*, **53**, 1072 (1982).
16. S. Wang, *Solid State Ionics*, **159**, 71 (2003).
17. G. D. T. Mahata, R.K. Mishra, B.P. Sharma, *Journal of Alloys and Compounds* **391**, 129 (2005).
18. S. P. Jiang, *Solid State Ionics* **146**, 1 (2002).
19. J. Nielsen, P. Hjalmarsson, M. H. Hansen and P. Blennow, *Journal of Power Sources*, **245**, 418 (2014).
20. S. B. Adler, J. A. Lane and B. C. H. Steele, *Journal of The Electrochemical Society*, **143**, 3554 (1996).
21. E. Siebert, A. Hammouche and M. Kleitz, *Electrochimica Acta*, **40**, 1741 (1995).
22. M. Izuki, M. E. Brito, K. Yamaji, H. Kishimoto, D.-H. Cho, T. Shimonosono, T. Horita and H. Yokokawa, *Journal of Power Sources*, **196**, 7232 (2011).